

Combined constraints on deviations of dark energy from an ideal fluid from Euclid and Planck

Elisabetta Majerotto¹*, Domenico Sapone² and Björn Malte Schäfer³

¹*Instituto de Física Teórica, Universidad Autónoma Madrid, C/ Nicols Cabrera 13-15, Cantoblanco, 28049 Madrid, Spain*

²*Cosmology and Theoretical Astrophysics group, Departamento de Física, FCFM, Universidad de Chile, Blanco Encalada 2008, Santiago, Chile*

³*Astronomisches Recheninstitut, Zentrum für Astronomie der Universität Heidelberg, Philosophenweg 12, 69120 Heidelberg, Germany*

30 August 2018

ABSTRACT

Cosmological fluids are commonly assumed to be distributed in a spatially homogeneous way, while their internal properties are described by a perfect fluid. As such, they influence the Hubble-expansion through their respective densities and equation of state parameters. The subject of this paper is an investigation of the fluid-mechanical properties of a dark energy fluid, which is characterised by its sound speed and its viscosity apart from its equation of state. In particular, we compute the predicted spectra for the integrated Sachs-Wolfe effect for our generalised fluid, and compare them with the corresponding predictions for weak gravitational lensing and galaxy clustering, which had been computed in previous work. We perform statistical forecasts and show that the integrated Sachs-Wolfe signal obtained by cross correlating Euclid galaxies with Planck temperatures, when joined to galaxy clustering and weak lensing observations, yields a percent sensitivity on the dark energy sound speed and viscosity. We prove that the iSW effect provides strong degeneracy breaking for low sound speeds and large differences between the sound speed and viscosity parameters.

Key words: cosmology: weak gravitational lensing, cosmic microwave background, methods: analytical

1 INTRODUCTION

The expansion dynamics of the Universe is usually described by assuming (i) general relativity as the theory of gravity, (ii) a high degree of symmetry, namely spatial isotropy and homogeneity at each instant in time, and (iii) ideal fluids which source the gravitational fields. These three assumptions lead to the Friedmann-equations for the time-evolution of the scale factor $a(t)$, which reflect the fact that Einstein’s field equation is of second order, and shows acceleration or deceleration \ddot{a} as phenomena.

The inclusion of the cosmological constant on grounds of the Lovelock theorem, which states that the field equation is the most general one in four dimensions, which includes derivatives of the metric of up to second order, and which conserves energy-momentum, yields a natural way to explain cosmic acceleration at late times.

Introducing dynamic dark energy components based on scalar self-interacting fields and interpreting the energy-momentum-tensor with the corresponding conservation law allows the identification of the homogeneous and isotropic field with a relativistic ideal fluid, whose relation between pressure and density is parametrized by an equation of state $w = p/\rho$. At the same time, this equation of state is the only free function that is allowed by

the Einstein field equation with the symmetry assumptions of the Robertson-Walker metric.

For these reasons, a central goal of cosmology is to investigate dark energy and the cosmological constant through their influence on the dynamics of the scale factor and on the growth of structures. The fluid-picture is attractive due to its generality: Apart from actual substances like relativistic components ($w = +1/3$) and nonrelativistic components ($w = 0$), it is general enough to describe spatial curvature ($w = -1/3$) and the cosmological constant ($w = -1$), while isotropy and homogeneity of the fluid ensure the Friedmann-symmetries.

Dark energy models based on self-interacting scalar fields show a natural variation of the dark energy equation of state parameter, because their time-evolution is governed by the Klein-Gordon equation, and therefore the kinetic and potential terms in their energy-momentum tensor evolve, leading to a time evolution in the equation of state, and therefore to a variation of their influence on the expansion dynamics of the Universe. In the slow-roll limit one recovers values of w close to -1 , resulting in accelerated expansion.

Adopting the fluid picture is an important test of whether the dark energy fluid is ideal or not: If the fluid has inhomogeneities, pressure fluctuations and density fluctuations are related through a sound speed, which in the most straightforward case describes an adiabatic compression of the fluid, there can be anisotropic stresses,

* e-mail: elisabetta.majerotto@uam.es

and finally, velocity perturbations can experience viscous forces that dissipate kinetic energy (for literature in this field we refer to Battye & Moss 2006; Mota et al. 2007; Battye & Moss 2009; Calabrese et al. 2011; Ballesteros et al. 2012; Sapone & Majerotto 2012; Sapone et al. 2013; Appleby et al. 2013; Dossett & Ishak 2013; Sawicki et al. 2013; Amendola et al. 2014; Chang & Xu 2014; Chang et al. 2014; Cardona et al. 2014; Pearson 2014; Ballesteros 2015). In addition, there can be a nonlinear relation between pressure and density of a fluid, one example of which would be Chaplygin-cosmologies (Bento et al. 2002; Li & Xu 2014), while a similar phenomenology could in principle be due to modifications in gravity rather than due to non-ideal fluids under general relativity (Kunz & Sapone 2007; Bertschinger & Zukin 2008; Silvestri 2009; Pogosian et al. 2010; Song et al. 2010; Leon & Saridakis 2011; Saltas & Kunz 2011; Baker et al. 2013; Boubekur et al. 2014).

These modifications break homogeneity on small scales, and require corresponding fluid equations for their time evolution, as well as couplings to local gravitational fields, which enable interaction between the dark energy fluid, the dark matter and the baryonic component. Commonly, one observes a difference between the two metric potentials in the case of nonzero sound speeds and equations of state unequal to -1 , which can be probed by photons, relative to the motion of nonrelativistic objects such as galaxies, which is only sensitive to a single metric potential.

In this paper we investigate cosmological perturbations with a non-ideal dark energy fluid and aim to forecast constraints on its speed of sound c_s and its viscosity from Euclid¹ (Laureijs 2009; Laureijs et al. 2011) and Planck (Ade et al. 2014b, 2015). Specifically, we consider tomographic weak gravitational lensing (Ayaita et al. 2012), galaxy clustering (DeDeo et al. 2003; Takada 2006) and the integrated Sachs-Wolfe effect (Dossett & Ishak 2013; Sogergel et al. 2015) as probes on the influence of non-ideal fluids on the statistics and the evolution of structures, while the background expansion dynamics is given through the individual density parameters and the equation of state parameters, assuming that there is no energy exchange between the fluids.

Our work is complementary to that of Mota et al. (2007); Calabrese et al. (2011); Chang & Xu (2014), who used the same model to describe the evolution of anisotropic stress: Mota et al. (2007); Chang & Xu (2014) computed constraints on it from the Cosmic Microwave Background (CMB), the large scale structure and Supernovae Type Ia, while Calabrese et al. (2011) forecasted errors from the CMB on the parameters of an early dark energy possessing anisotropic stress. It is also complementary to that of Amendola et al. (2014); Cardona et al. (2014); Sawicki et al. (2013), who also put constraints on anisotropic dark energy, but used different models for its evolution.

Currently, there are no significant deviations from dark energy being a perfect fluid, for instance the result by (Bean & Doré 2004) who find $c_s^2 < 0.04$ at low significance from CMB-data, such that tests whether dark energy is an ideal fluid will be the domain of future experiments: Quite generally, the sensitivity to non-ideal cosmic fluids requires their respective density to be large enough and their equation of state not to be too negative for dark energy perturbations to be sufficiently strong (Erickson et al. 2002; Koivisto & Mota 2006; de Putter et al. 2010; Ballesteros & Lesgourgues 2010; Archidiacono et al. 2014). At a first sight it would appear that choosing a dark energy equation of state too far from the cosmological constant value is incompatible with present constraints

(Ade et al. 2015). However, when including extra parameters such as the speed of sound and viscosities in the fluid, constraints become much more loose (Mota et al. 2007; Archidiacono et al. 2014, See e.g.).

This article is structured as follows: We develop the necessary perturbation equations for non-ideal dark energy fluids and a suitable parametrization in Sect. 2 and discuss cosmological probes in Sect. 3, before computing forecasts on non-ideal dark energy properties in Sect. 4. We summarise our results in Sect. 5. The reference cosmological model is a spatially flat, dark-energy dominated model with the parameter choices $\{\Omega_m h^2, \Omega_b h^2, n_s, \Omega_m\} = \{0.142, 0.022, 0.67, 0.96, 0.32\}$. This corresponds to the constraints from Planck (Ade et al. 2014b) and WMAP polarization low-multipole likelihood (Bennett et al. 2013; Ade et al. 2014a), and it represents the present official baseline for Euclid forecasts. The amplitude of the primordial power spectrum was fixed to $A_s = 2.1 \times 10^{-9}$. The dark energy equation of state parameter was set to be constant with a numerical value of $w = -0.8$.

2 COSMOLOGY WITH NON-IDEAL FLUIDS

2.1 Expansion dynamics

Since we focus on late cosmological times, where dark matter and dark energy are dominating the energy density of the Universe, we can approximate the Hubble function $H(a) = \dot{a}/a$ with

$$H^2 = H_0^2 \left[\Omega_{m,0} a^{-3} + (1 - \Omega_{m,0}) a^{-3(1+w)} \right], \quad (1)$$

where a is the scale factor, $\Omega_{m,0}$ is the dark matter density parameter today, w is the equation of state of dark energy, which we assume to be constant, and H_0 is the Hubble parameter today. In addition, we do not consider global curvature. The comoving distance is defined as

$$\chi = c \int_a^1 \frac{da}{a^2 H(a)} \equiv \chi_H \int_a^1 \frac{da}{a^2 H(a)/H_0}, \quad (2)$$

with the Hubble distance $\chi_H = c/H_0 \simeq 2996.9$ Mpc/h. At the same time, this defines conformal time τ through $\chi = c\tau$. In the following, we will set $c = 1$.

2.2 Perturbations and their analytical solutions

If we consider a non-ideal fluid dark energy, characterised by a constant equation of state w , a speed of sound c_s , and an anisotropic stress component σ , we can write the evolution of σ as in Hu (1998):

$$\sigma' + \frac{3}{a}\sigma = \frac{8}{3} \frac{c_v^2}{(1+w)^2} \frac{V}{a^2 H}, \quad (3)$$

where the prime indicates derivative with respect to a and c_v^2 is called viscosity parameter, as it gives a measure of the fluid's viscosity: Indeed, Eq. (3) implies that when $c_v^2 = 0$, then the anisotropic stress component σ is also vanishing, while when e.g. $c_v^2 = 1/3$ the evolution of anisotropic stress for radiation up to the quadrupole is recovered.

To this equation, we add the first order perturbation equations for the density contrast δ and the velocity perturbation V

$$\delta' = 3(1+w)\phi' - \frac{V}{Ha^2} - 3\frac{1}{a} \left(\frac{\delta p}{\rho} - w\delta \right), \quad (4)$$

$$V' = -(1-3w)\frac{V}{a} + \frac{k^2}{Ha^2} \frac{\delta p}{\rho} + (1+w)\frac{k^2}{Ha^2} \psi + \quad (5)$$

¹ <http://www.euclid-ec.org/>

$$- (1+w) \frac{k^2}{Ha^2} \sigma,$$

where δp is the pressure perturbation, ρ is the dark energy density, ψ and ϕ are the metric perturbations in the Newtonian gauge, defined by the line element

$$ds^2 = a^2 \left[-(1+2\psi)d\tau^2 + (1-2\phi)dx_i dx^i \right]. \quad (6)$$

Pressure perturbations are parametrized as

$$\delta p = c_s^2 \rho \delta + \frac{3aH(c_s^2 - c_a^2)}{k^2} \rho V, \quad (7)$$

where $c_a^2 \equiv \dot{p}/\dot{\rho} = w$ is the adiabatic speed of sound for a fluid with constant equation of state, to which c_s^2 reduces in the case of a perfect fluid, when no dissipative effects, leading to entropic perturbations, are present (Bean & Doré 2004).

In order to close the differential equation system, one needs to include the Poisson equation

$$k^2 \phi = -4\pi G a^2 \sum_i \rho_i \left(\delta_i + \frac{3aH}{k^2} V_i \right) = -4\pi G a^2 \sum_i \rho_i \Delta_i, \quad (8)$$

(where the sum runs over all clustering fluids, G is the Newton constant, and in the last equality we have defined the gauge-invariant density perturbation of the i -th fluid, $\Delta_i \equiv \delta_i + 3aH V_i / k^2$) and the fourth Einstein equation

$$\begin{aligned} k^2 (\phi - \psi) &= 12\pi G a^2 (1+w) \rho \sigma \\ &= \frac{9}{2} H_0^2 (1 - \Omega_{m,0}) a^{-(1+3w)} (1+w) \sigma \\ &\equiv B(a) \sigma. \end{aligned} \quad (9)$$

In Sapone & Majerotto (2012) the following analytical solutions for δ , V and σ were found for the matter dominated era:

$$\delta = \frac{3(1+w)^2}{3c_s^2(1+w) + 8(c_s^2 - w)c_v^2} \frac{\phi_0}{k^2}, \quad (11)$$

$$\begin{aligned} V &= -\frac{9(1+w)^2(c_s^2 - w)}{3c_s^2(1+w) + 8c_v^2(c_s^2 - w)} H_0 \sqrt{\Omega_m} \frac{\phi_0}{\sqrt{ak^2}}, \\ &= -3aH(c_s^2 - w) \delta, \end{aligned} \quad (12)$$

$$\sigma = -\frac{8c_v^2(c_s^2 - w)}{3c_s^2(1+w) + 8(c_s^2 - w)c_v^2} \frac{\phi_0}{k^2}, \quad (13)$$

where $k^2 \phi \simeq -\phi_0$, which is valid strictly only during matter domination and while neglecting dark energy perturbations.

As found in Sapone & Majerotto (2012), to which we refer for further detail on the analytic solutions, the relevant quantity is the effective sound speed

$$c_{\text{eff}}^2 = c_s^2 + \frac{8}{3} c_v^2 \frac{c_s^2 - w}{1+w}, \quad (14)$$

as Eqs. (11-13) can be rewritten in terms of it. This means that the sound speed and the viscosity have a similar damping effect on density and velocity perturbations (as also noticed in Mota et al. 2007; Calabrese et al. 2011). It is interesting to notice that the effect of c_v^2 is enhanced with respect to that of c_s^2 by a factor of $8(c_s^2 - w)/[3(1+w)]$, which is ~ 10 if $w \sim -0.8$ and for very small c_s^2 , which are the cases where a viscosity can be observed best, as will be shown in the following sections, and bounded by the case of a cosmological constant, as Eq. (11) diverges for $w = -1$.

2.3 Observable parameters

To understand how the viscosity affects the physical observables, it is useful to introduce the clustering parameter Q and the anisotropy parameter η , defined in Amendola et al. (2008) and computed in the case of viscous dark energy in Sapone & Majerotto (2012).

Q parametrizes the deviation from a purely matter-dominated Newtonian potential and is given by (see Sapone & Majerotto 2012)

$$\begin{aligned} Q - 1 &\equiv \frac{\rho \Delta}{\rho_m \Delta_m} = \frac{1 - \Omega_{m,0}}{\Omega_{m,0}} (1+w) \frac{a^{-3w}}{1 - 3w + \frac{2k^2 a}{3H_0^2 \Omega_{m,0}} c_{\text{eff}}^2} \\ &= Q_0 \frac{a^{-3w}}{1 + \alpha a}, \end{aligned} \quad (15)$$

where $\alpha = 2k^2 c_{\text{eff}}^2 / [(3H_0^2 \Omega_{m,0})(1 - 3w)]$ and $Q_0 = (1+w)(1 - \Omega_{m,0}) / [\Omega_{m,0}(1 - 3w)]$.

The anisotropy parameter is then given by

$$\eta \equiv \frac{\psi}{\phi} - 1 = -\frac{9}{2} H_0^2 (1 - \Omega_{m,0}) (1+w) \frac{a^{-1-3w}}{k^2 Q} \left(1 - \frac{c_s^2}{c_{\text{eff}}^2} \right). \quad (16)$$

This is nonzero only when anisotropic stress is present and the metric perturbations ϕ and ψ are different.

Let us finally define the parameter Σ (Amendola et al. 2008) as

$$\Sigma = \left(1 + \frac{1}{2} \eta \right) Q. \quad (17)$$

This is useful because it represents the deviation of the weak lensing potential $\Phi = \psi + \phi$ from its behaviour in the case of no dark energy perturbations.

3 COSMOLOGICAL PROBES

In Sapone et al. (2013), we forecasted constraints to the viscosity parameter and the sound speed from the Euclid galaxy clustering and weak lensing surveys. Here, we aim to complete the picture by adding to the latter the constraints from the iSW tomography signal obtained by cross-correlating galaxies mapped by the Euclid photometric instrument with the Planck temperature map: This provides a combination of all major probes of cosmic structure formation, which draw their sensitivity from the growth rate and interactions between fluids, from the shape of the initial perturbations and from the expansion history.

The Euclid survey is a mission of the ESA Cosmic Vision program that will be launched in 2020, and will perform both a photometric and a spectroscopic survey, the first aiming mainly at measuring weak lensing while the second at measuring the galaxy power spectrum. The Planck satellite is also a mission of ESA Cosmic Vision program, already operating and mapping the CMB fluctuations with unprecedented precision and control of systematic effects.

To perform our forecasts we use the Fisher matrix (Tegmark et al. 1997), which quantifies the decrease in likelihood if a model parameter θ_a moves away from the fiducial value, and can be computed for a local Gaussian approximation to the likelihood $\mathcal{L} \propto \exp(-\chi^2/2)$. In our forecasts we assume the official Euclid specifications, that can be found in Laureijs et al. (2011). The fiducial cosmological parameters correspond to the 2013 Planck measurements (Ade et al. 2014b), except for the value of w , for which we assume $w = -0.8$, in order for the effects to be more clearly visible (as done in Sapone & Majerotto 2012; Sapone et al. 2013) and of course except for the values of c_s^2 and c_v^2 .

In the following, we will describe the iSW tomography signal and give a short summary on the signal coming from weak lensing and the galaxy power spectrum from spectroscopy.

3.1 iSW signal

When a CMB photon moves into a time-evolving metric such as that of Eq. (6) the unbalance between the blue-shift experienced at the entrance and the red-shift experienced at the exit of its varying potential well originates a perturbation ζ in the CMB temperature T_{CMB} given by (Sachs & Wolfe 1967),

$$\zeta = \frac{\Delta T}{T_{\text{CMB}}} \equiv \int d\tau \left(\frac{\partial \Phi}{\partial \tau} + \frac{\partial \psi}{\partial \tau} \right) = \int_0^{\chi_H} d\chi a^2 H \frac{\partial \Phi}{\partial a}, \quad (18)$$

where χ is the comoving distance (see Eq. 2) and Φ is the weak lensing potential.

In the case of pure matter domination, $\Phi = \text{const}$, hence the iSW effect vanishes, while in presence of any fluid with $w \neq 0$ the temperature fluctuation ζ will be nonzero, so that the late iSW is particularly interesting to us, as it is originated by the appearing of dark energy and it is an independent proof of its existence (first detected by Boughn & Crittenden 2004; Giannantonio et al. 2012, for an updated measurement).

Let us now compute the term inside the integral, passing to Fourier space, and in the case of viscous dark energy (see also Sapone & Majerotto 2012; Schaefer 2009):

$$\begin{aligned} \frac{\partial \Phi}{\partial a} = & -\frac{3}{2} \frac{H_0^2 \Omega_{m,0}}{a k^2} \left\{ \Sigma(a, k) \Delta'_m(a, k) + \right. \\ & \left. + \Sigma'(a, k) \Delta_m(a, k) - \frac{1}{a} \Sigma(a, k) \Delta_m(a, k) \right\}. \end{aligned} \quad (19)$$

It is possible to see from this expression that anisotropic perturbations enter the iSW effect in two ways: by modifying Δ_m and through the additional presence of Σ and Σ' . At linear order, it is possible to isolate today's Δ_m from its time evolution:

$$\Delta_m(a, k) = a G(a, k) \Delta_{m,0}(k), \quad (20)$$

where $\Delta_{m,0}(k) \equiv \Delta_m(a=1, k)$. We write hence Eq. (19) as:

$$\frac{\partial \Phi}{\partial a} = -\frac{3}{2} \frac{H_0^2 \Omega_{m,0}}{k^2} \frac{\partial}{\partial a} \left\{ G(a, k) \Sigma(a, k) \right\} \Delta_{m,0}(k), \quad (21)$$

and Eq. (18) reads now

$$\zeta = \int_0^{\chi_H} d\chi W_\zeta(\chi) \Delta_{m,0}(k) \quad (22)$$

where the weighting function $W_\zeta(\chi)$ is

$$W_\zeta(\chi) = \frac{3}{2} \frac{H_0^2 \Omega_{m,0}}{k^2} a^2 H \frac{\partial}{\partial a} \left\{ G(a, k) \Sigma(a, k) \right\}. \quad (23)$$

Since the iSW is a secondary effect of the CMB (Rees & Sciama 1968), it can be separated through cross-correlation to the galaxy density (Crittenden & Turok 1996). Let us hence write the galaxy density obtained through imaging surveys, in order to compute its cross-correlation with the iSW. The line-of-sight projected galaxy density γ is given by (Smail et al. 1995)

$$\gamma = \int_0^{\chi_H} d\chi D(z) \frac{dz}{d\chi} b(\chi) G(\chi) \delta(z) \quad (24)$$

being $D(z)$ the galaxy distribution defined as

$$D(z) = \left(\frac{z}{z_0} \right)^2 \exp \left[- \left(\frac{z}{z_0} \right)^{\beta_D} \right], \quad (25)$$

where the fiducial parameters β_D and z_0 depend on the imaging survey considered. In the case of Euclid, they are $\beta_D = 3/2$, $z_0 = z_{\text{mean}} / \sqrt{2}$, and $z_{\text{mean}} = 0.9$ (Laureijs et al. 2011).

Even though the signal from the iSW increases noticeably when cross-correlating it with the galaxy density field, both the cross-correlation spectrum and the galaxy spectrum are line-of-sight integrated quantities, hence much information may be lost. For this reason we decide to use iSW tomography (Ho et al. 2008; Douspis et al. 2008; Juergens & Schaefer 2012), and in particular we divide the whole galaxy sample into 5 bins with equal number of galaxies (in order to match with the binning used by official Euclid documents for weak lensing tomography). To do this, we replace the galaxy distribution function $D(z)$, Eq. (25) in γ , Eq. (24), with the radial distribution function of galaxies in the i -th bin $D_i(z)$, obtained by binning the overall distribution $D(z)$ and convolving it with the photometric redshift distribution function (Amendola et al. 2008).

We are finally able to write our observable, i.e. the iSW-galaxy cross-correlation spectrum $C_{\zeta\gamma,i}(\ell)$ in the i -th redshift bin, along with the iSW-auto correlation spectrum $C_{\zeta\zeta}(\ell)$ and the galaxy-galaxy auto correlation spectrum $C_{\gamma\gamma,ij}(\ell)$ of the ij -bins, (which are both needed in order to estimate statistical errors coming from $C_{\zeta\zeta}(\ell)$), by applying a Limber-projection (Limber 1954) in the flat-sky approximation:

$$C_{\zeta\gamma,i}(\ell) = \int_0^{\chi_H} \frac{d\chi}{\chi^2} W_\zeta(\chi) W_{\gamma,i}(\chi) P_{\Delta\Delta}(k = \ell/\chi), \quad (26)$$

$$C_{\zeta\zeta}(\ell) = \int_0^{\chi_H} \frac{d\chi}{\chi^2} W_\zeta^2(\chi) P_{\Delta\Delta}(k = \ell/\chi) \quad (27)$$

$$C_{\gamma\gamma,ij}(\ell) = \int_0^{\chi_H} \frac{d\chi}{\chi^2} W_{\gamma,i}(\chi) W_{\gamma,j}(\chi) P_{\Delta\Delta}(k = \ell/\chi) \quad (28)$$

where $\bar{P}_{\Delta\Delta}(k)$ is the linear matter power spectrum today, and the galaxy weighting function of the i -th bin $W_{\gamma,i}(\chi)$ is

$$W_{\gamma,i}(\chi) = D_i(z) \frac{dz}{d\chi} b(\chi) G(\chi). \quad (29)$$

The tomographic iSW spectra $C_{\zeta\gamma,i}(\ell)$ are shown in Fig. 1 for two fiducial models: a standard dark energy model with $c_s^2 = 1$ and $c_v^2 = 0$ (solid lines) and a model with viscosity: $c_s^2 = 10^{-5}$ and $c_v^2 = 10^{-6}$ (dashed lines), where the colour shading indicates the redshift bin for which $C_{\zeta\gamma,i}(\ell)$ was evaluated. The iSW-effect is a large-scale effect originating from low redshift, as the influence of dark energy on the growth of gravitational potentials in the large-scale structure is strongest. The effect of dark energy viscosity and small sound speed is strongest on large scales as well (see also Sapone & Majerotto 2012), and affects a wide range of multipoles. Keeping all cosmological parameters fixed, dark energy viscosity would increase the amplitude of the iSW-effect by up to 25% on large angular scales and at low redshift. This sensitivity of the spectra at low multipoles is fortunate because these scales can be well probed with the iSW-effect.

3.2 Weak Lensing

To the iSW tomography signal we add the weak lensing tomographic signal (Hu 1999, 2002; Heavens 2003; Jain & Taylor 2003), coming from the same photometric survey as γ and using the same redshift bins. Here, we only give the main equation expressing the weak lensing power spectrum, which is used for our forecasts, and refer to Sapone et al. (2013) for further details.

In presence of anisotropic stress, the weak lensing conver-

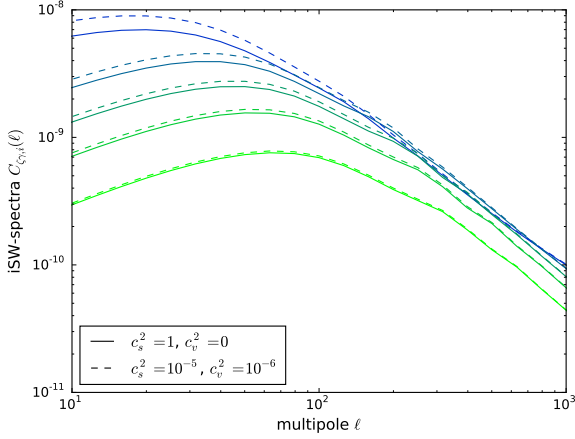


Figure 1. Tomographic iSW-spectra $C_{\gamma,i}(\ell)$ for two dark energy models: $c_s^2 = 1$ and $c_v^2 = 0$ as well as $c_s^2 = 10^{-5}$, $c_v^2 = 10^{-6}$. Blue to light green lines correspond to redshifts z in the intervals $[0.01 - 0.5595]$ (blue), $[0.5595 - 0.7871]$, $[0.7871 - 1.0165]$, $[1.0165 - 1.3184]$ and finally $[1.3184 - 2.5]$ (green).

gence power spectrum is given by (Jain & Taylor 2003; Hu 2002, 1999; Hu & Jain 2004)

$$C_{\kappa,ij}(\ell) = \int_0^{\chi_H} \frac{d\chi}{\chi^2} W_{\kappa,i}(\chi) W_{\kappa,j}(\chi) \Sigma^2 P_{NL}(k = \ell/\chi, \chi). \quad (30)$$

where the subscript ij refers to the redshift bins around z_i and z_j , with

$$W_{\kappa,i}(\chi) = \frac{3\Omega_m}{2\chi_H^2} \frac{F_i(\chi)}{a} \chi \quad (31)$$

$$F_i(\chi) = \int_{\chi}^{\chi_H} d\chi' n(\chi') D_i(\chi') \frac{\chi' - \chi}{\chi'} \quad (32)$$

and where D_i is the same tomographic distribution function of galaxies used for the iSW-effect. While tomography in general greatly reduces statistical errors the actual shape of the choice of the binning does not affect results in a serious way, although in principle there is room for optimisation (Schäfer & Heisenberg 2012).

In Fig. 2 we show the tomographic weak lensing spectra $C_{\kappa,ii}(\ell)$ for the same models and the same redshifts as in Fig. 1. As for iSW, the effect of viscosity is detected at large scales and for a large range of scales (but smaller than for iSW). Instead, contrarily to iSW, here the sensitivity to viscosity is stronger at higher redshift. This is because the efficiency of weak lensing is higher for longer light paths.

In principle it is also possible to define a cross-spectrum of weak lensing and iSW, $C_{\gamma,i}(\ell)$, and of weak lensing and galaxy distribution, $C_{\kappa,i}(\ell)$, but both these spectra are subdominant with respect to $C_{\gamma,i}(\ell)$. This is because the weak lensing convergence signal comes from the distortion of the light path at redshifts intermediate between us and the galaxies mapped by the imaging survey, while the iSW signal originates precisely at the same redshifts where the galaxies are. We have tested this fact by computing the signal to noise-ratio for measuring $C_{\kappa,i}(\ell)$ and found it much smaller than that of $C_{\gamma,i}(\ell)$.

3.3 Spectroscopic galaxy power spectrum

To the iSW and weak lensing measurements, both measured through photometric observations, we add data coming from the

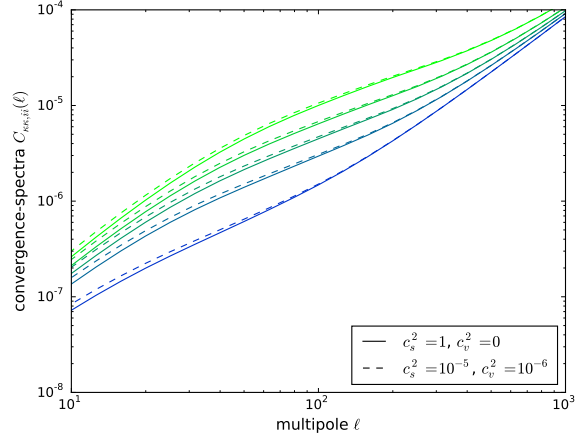


Figure 2. Tomographic weak lensing spectra $C_{\kappa,ii}(\ell)$ for two dark energy models, $c_s = 1$ and $c_v = 1$ as well as $c_s = 10^{-5}$, $c_v = 10^{-6}$, both including the shape noise term. Blue to light green lines correspond to the same redshift binning as in Fig. 1: $[0.01 - 0.5595]$ (blue), $[0.5595 - 0.7871]$, $[0.7871 - 1.0165]$, $[1.0165 - 1.3184]$ and finally $[1.3184 - 2.5]$ (green).

power spectrum of spectroscopically observed galaxies. Here we only show the expression of the observed power spectrum, which is needed in order to compute our forecasts, and refer again the reader to Sapone et al. (2013) for further detail.

Following Seo & Eisenstein (2003) we write the observed galaxy power spectrum as:

$$P_{\gamma\gamma}^{\text{spec}}(z, k_r, \mu_r) = \frac{D_A^2(z)H(z)}{D_A^2(z)H_r(z)} G^2(z, k) b(z)^2 (1 + \beta\mu^2)^2 P_{0r}(k) + P_{\text{shot}}, \quad (33)$$

where the subscript r refers to the reference (or fiducial) cosmological model.

Here P_{shot} is a scale-independent offset due to imperfect removal of shot-noise, $\mu = \vec{k} \cdot \hat{r}/k$, is the cosine of the angle of the wave mode with respect to the line of sight pointing into the direction \hat{r} , P_{0r} is the fiducial matter power spectrum evaluated at redshift zero, $G(z, k)$ is the linear growth factor of the matter perturbations, $b(z)$ is the bias factor and $D_A(z)$ is the angular diameter distance. The wavenumber k and μ have also to be written in terms of the fiducial cosmology (see Seo & Eisenstein 2003; Amendola et al. 2005; Sapone & Amendola 2007, for more details). The fiducial bias used can be found in Orsi et al. (2010), who derived their results by using a semi-analytical model of galaxy formation, while the matter power spectrum has been computed with a modified version of the CAMB code² (Lewis et al. 2000) accounting for anisotropies.

4 STATISTICAL ERRORS FORECASTS

In this section we estimate marginalised statistical errors on the sound speed and viscosity parameters c_s^2 and c_v^2 through the Fisher-matrix formalism (Tegmark et al. 1997), which assumes a Gaussian likelihood and unbiased measurements.

² <http://camb.info>

4.1 iSW Fisher matrix

The sensitivity of line of sight-integrating effects can be boosted by subdividing the galaxy population into redshift bins: For the iSW-effect this was first carried out successfully by [Ho et al. \(2008\)](#), and systematically investigated by [Juergens & Schaefer \(2012\)](#).

The Fisher-matrix of the iSW-effect follows directly from the variance of the spectrum estimates,

$$F_{\alpha\beta}^{\text{iSW}} = \sum_{\ell} \frac{\partial \bar{C}_{\zeta\gamma,i}(\ell)}{\partial \theta_{\alpha}} \text{Cov}_{ij}^{-1}(\ell) \frac{\partial \bar{C}_{\zeta\gamma,j}(\ell)}{\partial \theta_{\beta}} \quad (34)$$

where the sum runs from $\ell = 5$ to $\ell = 300^3$, θ_{α} are the cosmological parameters, $\text{Cov}_{ij}(\ell)$ is the covariance of the spectrum $\bar{C}_{\zeta\gamma,i}(\ell)$ and is given by

$$\text{Cov}_{ij}(\ell) = \frac{1}{2\ell + 1} \frac{1}{f_{\text{sky}}} \left[\bar{C}_{\zeta\gamma,i} \bar{C}_{\zeta\gamma,j}(\ell) + \bar{C}_{\zeta\zeta}(\ell) \bar{C}_{\gamma\gamma,ij}(\ell) \right], \quad (35)$$

and where quantities with the bar represent the estimate of the signal, including intrinsic CMB fluctuations, instrumental noise and the beam of the CMB experiment as noise sources:

$$\bar{C}_{\zeta\gamma,i}(\ell) = C_{\zeta\gamma,i}(\ell) \quad (36)$$

$$\bar{C}_{\zeta\zeta}(\ell) = C_{\zeta\zeta}(\ell) + C_{\text{CMB}}(\ell) + w_T^{-1} B^{-2}(\ell) \quad (37)$$

$$\bar{C}_{\gamma\gamma,ij}(\ell) = C_{\gamma\gamma,ij}(\ell) + \frac{\delta_{ij}}{n_i} \quad (38)$$

For Planck's noise levels, $w_T^{-1} = (0.02\mu\text{K})^2$ has been used and the beam was assumed to be Gaussian, $B^{-2}(\ell) = (2 \times 10^{-8})^2 \exp[\Delta\theta^2 \ell(\ell + 1)]$, with FWHM-width of $\Delta\theta = 7'.1$, corresponding to channels of Planck closest to the CMB-maximum at ~ 160 GHz. n_i is the number of galaxies per steradian in the tomography bin i . We assume uncorrelated noise terms, and as a consequence the cross-spectra $C_{\zeta\gamma,i}(\ell)$ are unbiased estimates of the actual spectra, see Eq. (36). The spectrum $C_{\text{CMB}}(\ell)$ of the CMB primary anisotropies from Planck has been computed with the CAMB code.

4.2 Weak Lensing Fisher matrix

The Fisher matrix for weak lensing is given by:

$$F_{\alpha\beta}^{\text{WL}} = f_{\text{sky}} \sum_{\ell} \frac{(2\ell + 1)}{2} \frac{\partial C_{\kappa\kappa,ij}(\ell)}{\partial \theta_{\alpha}} \bar{C}_{jk}^{-1}(\ell) \frac{\partial C_{\kappa\kappa,km}(\ell)}{\partial \theta_{\beta}} \bar{C}_{mi}^{-1}(\ell) \quad (39)$$

where the sum runs from $\ell = 5$ to $\ell = 5000$, (as from the official Euclid prescriptions, see [Laureijs et al. 2011](#)), and where the sum over repeated indices is implied. We added a Poissonian shape noise term to the weak lensing spectra,

$$\bar{C}_{\kappa\kappa,ij}(\ell) = C_{\kappa\kappa,ij}(\ell) + \delta_{ij} \frac{\langle \gamma_{\text{int}}^{1/2} \rangle}{n_i}, \quad (40)$$

γ_{int} is the rms intrinsic shear (here, we assume $\langle \gamma_{\text{int}}^{1/2} \rangle = 0.22$) and n_i is the number of galaxies per steradians belonging to the i -th bin. We assume a Gaussian shape of the covariance while noting that non-Gaussian contribution can have a strong influence on the derived forecasts ([Takada & Jain 2009](#)).

³ The integration range for the iSW-effect as well as the details of instrumental noise and angular resolution are not very important, as most of the signal is at low ℓ below $\ell \sim 100$, due to the large cosmic variance provided by the primary CMB fluctuations, which is the largest source of noise.

4.3 Spectroscopic galaxy distribution Fisher matrix

The galaxy power spectrum Fisher matrix is given by ([Seo & Eisenstein 2003](#))

$$F_{\alpha\beta}^{\text{GC}} = \int_{k_{\text{min}}}^{k_{\text{max}}} \frac{k^2 dk}{4\pi^2} \frac{\partial \ln P_{\gamma\gamma}^{\text{spec}}(z; k, \mu)}{\partial \theta_{\alpha}} \frac{\partial \ln P_{\gamma\gamma}^{\text{spec}}(z; k, \mu)}{\partial \theta_{\beta}} \times V_{\text{eff}}, \quad (41)$$

where GC stays for galaxy clustering, the observed galaxy power spectrum $P_{\gamma\gamma}^{\text{spec}}$ is given by Eq. (33), the derivatives are evaluated at the parameter values of the fiducial model, $k_{\text{min}} = 0.001$ and k_{max} is such that the rms amplitude of the fluctuations at the corresponding scale $R_{\text{max}} = 2\pi/k_{\text{max}}$ is $\sigma^2(R_{\text{max}}) = 0.25$, with an additional cut at $k_{\text{max}} = 0.2 h/\text{Mpc}$, in order to remain in the linear regime, V_{eff} is the effective volume of the survey, given by

$$V_{\text{eff}} \simeq \left(\frac{\bar{n} P_{\gamma\gamma}^{\text{spec}}(k, \mu)}{\bar{n} P_{\gamma\gamma}^{\text{spec}}(k, \mu) + 1} \right)^2 V_{\text{survey}}, \quad (42)$$

the latter equation holding for an average comoving number density \bar{n} . The number densities and further fiducial Euclid specifications can be found in [Laureijs et al. \(2011\)](#), [Majerotto et al. \(2012\)](#).

4.4 Forecasts

We computed forecasts on the measurement of c_s^2 and c_v^2 for a wide range of fiducial values, in order to capture the parameter determining capability of both experiments for a previously unknown set of parameters. The probes are assumed to be uncorrelated as discussed above, hence their Fisher-matrices add,

$$F_{\alpha\beta} = F_{\alpha\beta}^{\text{GC}} + F_{\alpha\beta}^{\text{WL}} + F_{\alpha\beta}^{\text{iSW}}, \quad (43)$$

and we derive confidence contours on c_s^2 and c_v^2 and individual errors from this combined Fisher-matrix, marginalising over all other five parameters considered in this analysis. $F_{\alpha\beta}^{\text{GC}}$ has been further marginalised over P_{shot} , while the galaxy bias has been kept fixed.

Our forecasts on the following fiducial models: $\{c_s^2, c_v^2\} = \{1, 0\}$, $\{10^{-3}, 10^{-4}\}$, $\{10^{-5}, 10^{-6}\}$ and $\{10^{-6}, 10^{-6}\}$ are shown in Figs. 3, 4, 5 and 6, respectively. The first model corresponds to the case of simple scalar field dark energy, while the following two pairs of fiducial models were chosen such that $c_s^2 = 10 c_v^2$ because, as mentioned previously in Sec. 2.2, the relevant quantity is the effective sound speed, and the effect of c_v^2 in it is ~ 10 times stronger than that of c_s^2 when $w = -0.8$ because of the factor multiplying c_v^2 in Eq. (14). The last model, also having small c_s^2 and c_v^2 , does not verify the latter relation, and has been chosen in order to be compared to previous work ([Sapone et al. 2013](#)) and to the similar case $\{c_s^2, c_v^2\} = \{10^{-5}, 10^{-6}\}$.

In all plots, iSW constraints are shown in blue, weak lensing ones in dark blue, GC ones in green, combined iSW-GC ones in yellow, combined iSW-weak lensing ones in orange, and combined iSW-GC-weak lensing ones in red.

From Figs. 3-6 it is clear that the results depend very much on the chosen fiducial model. A common feature is that iSW on its own does not provide very strong constraints. In particular (see also Tab. 1), c_v^2 is quite badly constrained, with relative errors ranging between 6.1×10^4 and 1.1×10^5 , while relative errors on c_s^2 are much smaller: between 1.1×10^{-1} and 1.4×10 . This was to be expected since the iSW-effect along has a rather small signal strength of about 5σ for cross-correlating the CMB with the Euclid galaxy sample ([Douspis et al. 2008](#)).

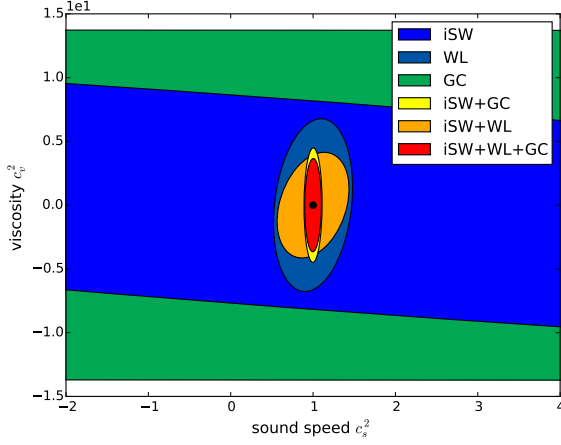


Figure 3. Forecasted 1σ -constraints on c_s^2 and c_v^2 for individual probes and all possible combinations, for the fiducial choice $c_s^2 = 1$ and $c_v^2 = 0$.

	c_s^2	c_v^2	$\sigma_{c_s^2/c_s^2}$	$\sigma_{c_v^2/c_v^2}$
iSW	1	0	1.4×10	$\sigma_{c_v^2} = 8.6$
	10^{-3}	10^{-4}	1.4×10	6.1×10^4
	10^{-5}	10^{-6}	1.4×10^{-1}	1.1×10^5
	10^{-6}	10^{-6}	4.0×10^2	4.4×10
WL	1	0	3.2×10^{-1}	$\sigma_{c_v^2} = 4.5$
	10^{-3}	10^{-4}	1.6×10^2	1.4×10^2
	10^{-5}	10^{-6}	3.7×10	3.5×10
	10^{-6}	10^{-6}	7.1	8.9×10^{-1}
GC	1	0	1.1×10^2	$\sigma_{c_v^2} = 9.1$
	10^{-3}	10^{-4}	7.5×10^{-2}	7.2×10^{-2}
	10^{-5}	10^{-6}	2.2	1.9
	10^{-6}	10^{-6}	4.7	1.2
iSW+WL	1	0	2.9×10^{-1}	$\sigma_{c_v^2} = 2.7$
	10^{-3}	10^{-4}	2.5×10^{-1}	5.6
	10^{-5}	10^{-6}	2.6×10^{-2}	7.5×10^{-1}
	10^{-6}	10^{-6}	7.0	7.6×10^{-1}
iSW+GC	1	0	7.2×10^{-2}	$\sigma_{c_v^2} = 3.0$
	10^{-3}	10^{-4}	5.3×10^{-2}	5.5×10^{-2}
	10^{-5}	10^{-6}	1.6×10^{-2}	1.2
	10^{-6}	10^{-6}	3.9	4.2×10^{-1}
GC+WL	1	0	6.7×10^{-2}	$\sigma_{c_v^2} = 3.7$
	10^{-3}	10^{-4}	7.4×10^{-2}	7.1×10^{-2}
	10^{-5}	10^{-6}	1.9	1.7
	10^{-6}	10^{-6}	3.5	4.8×10^{-1}
all	1	0	6.7×10^{-2}	$\sigma_{c_v^2} = 2.4$
	10^{-3}	10^{-4}	4.5×10^{-2}	4.5×10^{-2}
	10^{-5}	10^{-6}	1.2×10^{-2}	6.1×10^{-1}
	10^{-6}	10^{-6}	3.3	3.4×10^{-1}

Table 1. Relative errors on the parameters c_s^2 and c_v^2 from iSW, weak lensing and GC alone, from the combination of iSW and WL, iSW and GC, GC and WL, and from all three datasets. For the case $c_v^2 = 0$ the absolute error $\sigma_{c_v^2}$ is given.

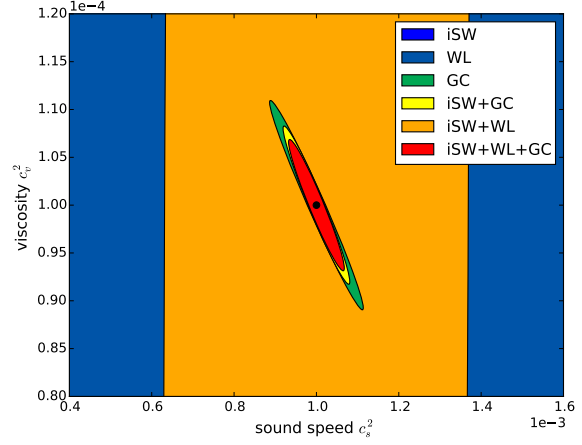


Figure 4. Forecasted 1σ -constraints on c_s^2 and c_v^2 for individual probes and all possible combinations, for the fiducial choice $c_s^2 = 10^{-3}$ and $c_v^2 = 10^{-4}$.

Weak lensing constraints⁴ are much stronger than iSW ones in the case of a fiducial scalar field dark energy, but become progressively comparable to them when the fiducial c_s^2 and c_v^2 become smaller, with the exception of the case $c_s^2 = c_v^2 = 10^{-6}$.

Even though both iSW and weak lensing do not give very strong constraints on sound speed and viscosity (see also Tab 1), it is very interesting to notice that the two data sets complement each other very well. This is especially true for the case $c_s^2 = 10^{-5}$ and $c_v^2 = 10^{-6}$, represented in Fig. 5, where the blue ellipses, which indicate errors from iSW, have a very different degeneration direction with respect to the dark blue contours, corresponding to errors from weak lensing, but are comparable to them in size. Therefore the resulting combined errors are much smaller than those from a single dataset. In particular, the iSW effect gives better constraints on the sound speed and weak lensing on the viscosity parameter.

Also, in the case of Figs. 3, 4 and 6 iSW and weak lensing have different degeneracies, but here joining them does not improve the errors significantly because the weak lensing effect gives stronger constraints on both parameters. Here, the improvement in combining the two probes is rather the multiplication of a constraining likelihood with a wide one, resulting nevertheless in an increase in peakiness.

Also errors on c_s^2 and c_v^2 from GC are orthogonal to those from the iSW, but only in the case where $c_s^2 = 10^{-5}$ and $c_v^2 = 10^{-6}$, see Fig. 5, this helps reducing the errors, because the former dataset performs better in constraining c_v^2 and the second c_s^2 . In the case of fiducial $c_s^2 = 10^{-3}$ and $c_v^2 = 10^{-4}$ it is GC which gives best errors on both parameters, while for the $c_s^2 = 1$ and $c_v^2 = 0$ fiducial model, it is weak lensing.

Another interesting question is whether iSW adds important information to that provided by the other two datasets, which had already been analysed in Sapone et al. (2013). Table 1 answers this question. It turns out that the information from iSW helps significantly in constraining c_s^2 and c_v^2 if the true model has $c_s^2 = 10^{-5}$ and $c_v^2 = 10^{-6}$, see Fig. 5. In this case the iSW alone gives a strong constraint, which has moreover a different degeneration direction with respect to the error from galaxy clustering and weak lensing.

⁴ With respect to Sapone et al. (2013) we have improved the estimation of P_{NL} by using the full CAMB output instead of an analytical approximation to it.

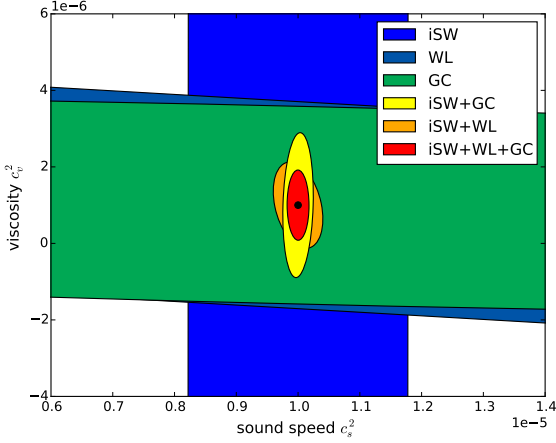


Figure 5. Forecasted 1σ -constraints on c_s^2 and c_v^2 for individual probes and all possible combinations, for the fiducial choice $c_s^2 = 10^{-5}$ and $c_v^2 = 10^{-6}$.

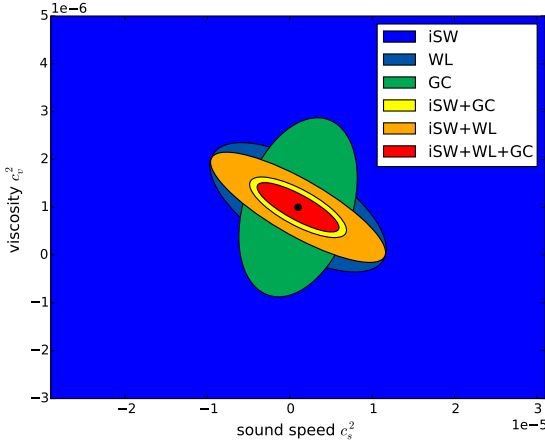


Figure 6. Forecasted 1σ -constraints on c_s^2 and c_v^2 for individual probes and all possible combinations, for the fiducial choice $c_s^2 = 10^{-6}$ and $c_v^2 = 10^{-6}$.

For the other three fiducial models the gain when adding iSW is not very strong, as in both cases the combination of weak lensing and galaxy clustering gives a much tighter constraint in both the sound speed and the viscosity than the iSW alone.

It is interesting to notice (see Fig. 6) that when both the sound speed and the viscosity are small, but the relation between c_s^2 and c_v^2 differs from $c_s^2 \sim 10c_v^2$, the iSW effect error ellipse becomes much larger and as a result the sound speed parameter is less strongly constrained. Thus we conclude that (i) very interesting results can be obtained through a combination from different cosmological probes and that (ii) the iSW-effect is able to tighten constraints significantly for cases where there is a large difference between c_s^2 and c_v^2 .

5 SUMMARY

In this paper we have investigated how well the viscosity and sound speed of dark energy can be measured with the iSW cross-correlation spectrum, when using Planck and Euclid observations,

and how joining iSW measurements to galaxy clustering and weak lensing ones improves constraints.

We found that the speed of sound is quite well constrained, with relative errors as small as 0.14 for small fiducial c_s^2 and c_v^2 , while relative errors on the viscosity parameter are very large. Even though the anisotropic stress is not well constrained by the iSW, the error ellipses are interestingly orthogonal to those from weak lensing, hence the combination of these two datasets constrains tightly the parameter space, giving relative errors on c_s^2 and c_v^2 as small as 2.6×10^{-2} and 7.5×10^{-2} respectively. This is an improvement of a factor ~ 1500 in the measurement of the sound speed and ~ 50 in the measurement of the viscosity parameter, with respect to the weak lensing only constraint. The improvement obtained when combining iSW with galaxy clustering is smaller: a factor of ~ 1.5 in c_s^2 and ~ 150 in c_v^2 . Finally, the addition of iSW to weak lensing and galaxy clustering constraints is most important if the fiducial sound speed and viscosity parameter are very small, while it is not very relevant for higher fiducial values of c_s^2 .

It is also important to remind that in order to make the effect of dark energy perturbations stronger we have always used a value of the equation of state parameter $w = -0.8$. For values close to $w = -1$ the effects on the observables due to the dark energy perturbations are reduced, as all the phenomenological functions used (such as $Q(k, a)$) have a term $\propto (1 + w)$. If we use a value of $w = -0.9$ we expect our final errors on the parameters to increase. But by how much? All the observables used in this paper depend most strongly on Q^2 (see Eq. 15) which is intrinsically included into the matter power spectrum; for a sound speed equal to zero $Q - 1 = (1 + w)/(1 - 3w)a^{-3w}$ so the relative increase of the errors on the sound speed will be given by $1/[Q(w = -0.9) - 1]/[Q(w = -0.8) - 1]^2$ which is of about a factor 4 larger, in agreement also with the results found in Sapone et al. (2010).

A detection of sound speed and viscosity different from the values associated to a classical scalar field, i.e. $c_s^2 = 1$ and $c_v^2 = 0$, will point to a new understanding of the accelerated phase of the Universe. This is because the non ideal fluid considered in this paper can be thought of as an effective dark energy fluid parametrizing a modified gravity model, see Kunz & Sapone (2007). In practice, the detection of a zero sound speed does not automatically mean that we are dealing with an actual dark energy fluid, even though one would nevertheless experience effects which could be attributed to fluctuations of a fluid.

In this paper we found that joining data from Euclid and Planck we are able to constrain simultaneously the sound speed and the viscosity parameters, provided that the two are sufficiently small. This is mostly due to the different sensitivity of the three observables, i.e. GC, WL and iSW to the two parameters. In most cases the iSW has a different degeneracy with respect to WL and GC, and this helps reducing the errors on c_s^2 and c_v^2 by a factor of ~ 100 (as pointed out before). Our results are in agreement with what found by Mota et al. (2007); Calabrese et al. (2011); Chang & Xu (2014), who show that for values of c_s^2 approaching $c_s^2 = 1$ the detection of a positive viscosity is very difficult, even when, as in the case of Calabrese et al. (2011), an early dark energy helps its detection by increasing its effect on smaller scales.

To conclude, are Euclid and Planck able to measure the sound speed and the viscosity parameters of a dark energy component? If the values of c_s^2 and c_v^2 are small enough, the answer is yes; consequently, we will be able to constrain well the effective dark energy model. On the contrary, if sound speed and viscosity will escape detection, at least one of the two parameters will likely have large

values. We would assume that other cosmological probes would not directly provide constraints on dark energy properties, but would nevertheless be able to provide constraining power by fixing other parts of the cosmological model, such as the dark matter density or the dark energy equation of state, which was not subject to variation in our investigation.

ACKNOWLEDGEMENTS

We acknowledge Martin Kunz and Luca Amendola for inspiring discussions.

E. M. was supported by the Spanish MINECO's "Centro de Excelencia Severo Ochoa"-programme under grant No. SEV-2012-0249 and by the Spanish MICINN's Juan de la Cierva programme (JCI-2010-08112), by CICYT through the project FPA-2012-31880, by the Madrid Regional Government (CAM) through the project HEPHACOS S2009/ESP-1473 under grant P-ESP-00346 and by the European Union FP7 ITN INVISIBLES (Marie Curie Actions, PITN- GA-2011- 289442). DS acknowledges financial support from the Fondecyt project number 11140496 and from the "Anillo" project ACT1122 founded by the "Programa de Investigación asociativa".

REFERENCES

- Ade P., et al., 2014a, *Astron.Astrophys.*, 571, A15
 Ade P., et al., 2014b, *Astron.Astrophys.*, 571, A16
 Ade P., et al., 2015, *ArXiv e-prints* 1502.01589
 Amendola L., Fogli S., Guarnizo A., Kunz M., Vollmer A., 2014, *Phys.Rev.*, D89, 063538
 Amendola L., Kunz M., Sapone D., 2008, *JCAP*, 0804, 013
 Amendola L., Quercellini C., Giallongo E., 2005, *Mon.Not.Roy.Astron.Soc.*, 357, 429
 Appleby S. A., Linder E. V., Weller J., 2013, *Phys.Rev.*, D88, 043526
 Archidiacono M., Lopez-Honorez L., Mena O., 2014, *Phys.Rev.*, D90, 123016
 Ayaita Y., Schäfer B. M., Weber M., 2012, *MNRAS*, 422, 3056
 Baker T., Ferreira P. G., Skordis C., 2013, *Phys. Rev. D*, 87, 024015
 Ballesteros G., 2015, *JCAP*, 1503, 001
 Ballesteros G., Hollenstein L., Jain R. K., Kunz M., 2012, *JCAP*, 1205, 038
 Ballesteros G., Lesgourgues J., 2010, *J. Cosmology Astropart. Phys.*, 10, 14
 Battye R., Moss A., 2009, *Phys.Rev.*, D80, 023531
 Battye R. A., Moss A., 2006, *Phys.Rev.*, D74, 041301
 Bean R., Doré O., 2004, *Phys. Rev. D*, 69, 083503
 Bennett C., et al., 2013, *Astrophys.J.Suppl.*, 208, 20
 Bento M., Bertolami O., Sen A., 2002, *Phys.Rev.*, D66, 043507
 Bertschinger E., Zukin P., 2008, *Phys.Rev.*, D78, 024015
 Boubekeur L., Giusarma E., Mena O., Ramírez H., 2014, *Phys. Rev. D*, 90, 103512
 Boughn S., Crittenden R., 2004, *Nature*, 427, 45
 Calabrese E., de Putter R., Huterer D., Linder E. V., Melchiorri A., 2011, *Phys.Rev.*, D83, 023011
 Cardona W., Hollenstein L., Kunz M., 2014, *JCAP*, 1407, 032
 Chang B., Lu J., Xu L., 2014, *Phys.Rev.*, D90, 103528
 Chang B., Xu L., 2014, *Phys.Rev.*, D90, 027301
 Crittenden R. G., Turok N., 1996, *Phys.Rev.Lett.*, 76, 575
 de Putter R., Huterer D., Linder E. V., 2010, *Phys. Rev. D*, 81, 103513
 DeDeo S., Caldwell R. R., Steinhardt P. J., 2003, *Phys. Rev. D*, 67, 103509
 Dossett J., Ishak M., 2013, *Phys.Rev.*, D88, 103008
 Douspis M., Castro P. G., Caprini C., Aghanim N., 2008, *A&A*, 485, 395
 Erickson J. K., Caldwell R. R., Steinhardt P. J., Armendariz-Picon C., Mukhanov V., 2002, *Physical Review Letters*, 88, 121301
 Giannantonio T., Crittenden R., Nichol R., Ross A. J., 2012, *Mon.Not.Roy.Astron.Soc.*, 426, 2581
 Heavens A., 2003, *Mon.Not.Roy.Astron.Soc.*, 343, 1327
 Ho S., Hirata C., Padmanabhan N., Seljak U., Bahcall N., 2008, *Phys. Rev. D*, 78, 043519
 Hu W., 1998, *Astrophys.J.*, 506, 485
 Hu W., 1999, *Astrophys.J.*, 522, L21
 Hu W., 2002, *Phys.Rev.*, D66, 083515
 Hu W., Jain B., 2004, *Phys.Rev.*, D70, 043009
 Jain B., Taylor A., 2003, *Phys.Rev.Lett.*, 91, 141302
 Juergens G., Schaefer B. M., 2012, *Mon.Not.Roy.Astron.Soc.*, 425, 2589
 Koivisto T., Mota D. F., 2006, *Phys.Rev.*, D73, 083502
 Kunz M., Sapone D., 2007, *Phys.Rev.Lett.*, 98, 121301
 Laureijs R., 2009, *ArXiv e-prints* 0912.0914
 Laureijs R., et al., 2011, *ArXiv e-prints* 1110.3193
 Leon G., Saridakis E. N., 2011, *Class.Quant.Grav.*, 28, 065008
 Lewis A., Challinor A., Lasenby A., 2000, *Astrophys.J.*, 538, 473
 Li W., Xu L., 2014, *Eur.Phys.J.*, C74, 2765
 Limber D. N., 1954, *Astrophys.J.*, 119, 655
 Majerotto E., Guzzo L., Samushia L., Percival W. J., Wang Y., et al., 2012, *Mon.Not.Roy.Astron.Soc.*, 424, 1392
 Mota D., Kristiansen J., Koivisto T., Groeneboom N., 2007, *Mon.Not.Roy.Astron.Soc.*, 382, 793
 Orsi A., Baugh C., Lacey C., Cimatti A., Wang Y., et al., 2010, *Mon.Not.Roy.Astron.Soc.*, 405, 1006
 Pearson J. A., 2014, *Annalen Phys.*, 526, 318
 Pogosian L., Silvestri A., Koyama K., Zhao G.-B., 2010, *Phys.Rev.*, D81, 104023
 Rees M., Sciama D., 1968, *Nature*, 217, 511
 Sachs R., Wolfe A., 1967, *Astrophys.J.*, 147, 73
 Saltas I. D., Kunz M., 2011, *Phys.Rev.*, D83, 064042
 Sapone D., Amendola L., 2007, *ArXiv e-prints* 0709.2792
 Sapone D., Kunz M., Amendola L., 2010, *Phys.Rev.*, D82, 103535
 Sapone D., Majerotto E., 2012, *Phys.Rev.*, D85, 123529
 Sapone D., Majerotto E., Kunz M., Garilli B., 2013, *Phys.Rev.*, D88, 043503
 Sawicki I., Saltas I. D., Amendola L., Kunz M., 2013, *J. Cosmology Astropart. Phys.*, 1, 4
 Schaefer B. M., 2009, *Mon.Not.Roy.Astron.Soc.*, 388, 1394
 Schäfer B. M., Heisenberg L., 2012, *MNRAS*, 423, 3445
 Seo H.-J., Eisenstein D. J., 2003, *Astrophys.J.*, 598, 720
 Silvestri A., 2009, *Nucl.Phys.Proc.Suppl.*, 194, 326
 Smail I., Hogg D. W., Blandford R., Cohen J. G., Edge A. C., et al., 1995, *Mon.Not.Roy.Astron.Soc.*, 277, 1
 Soergel B., Giannantonio T., Weller J., Battye R. A., 2015, *JCAP*, 1502, 037
 Song Y.-S., Hollenstein L., Caldera-Cabral G., Koyama K., 2010, *J. Cosmology Astropart. Phys.*, 4, 18
 Takada M., 2006, *Phys. Rev. D*, 74, 043505
 Takada M., Jain B., 2009, *MNRAS*, 395, 2065
 Tegmark M., Taylor A., Heavens A., 1997, *Astrophys.J.*, 480, 22

This paper has been typeset from a \TeX/L\TeX file prepared by the author.